PS/FES
Int. 68-1

THE DEVELOPMENT OF INCLINED SPARKS IN A TRACK-FOLLOWING SPARK CHAMBER

C.J. Evans*

Contents :

* Visitor from the Department of Physics, University College of Swansea.

PS/6353
19 February, 1968

ABSTRACT

This report describes a theoretical investigation into the phenomenon of electrical break-down along particle trajectories in a wide gap spark chamber. The differential equations for ionization growth, written in a form which allows for the space-charge effects of a number of adjacent electron avalanches, are solved numerically using a second-order iterative method. The results show that the development of the inclined spark can be explained on the basis of known values of the primary ionization coefficient, electron drift velocity and diffusion coefficient. Some results for a single avalanche are also given for comparison.

1. INTRODUCTION

This report deals with theoretical aspects of spark formation along the trajectories of nuclear particles, as is characteristic of the spark mode of operation of a wide-gap spark chamber. Experiments have shown that track-following takes place even for tracks inclined at large angles to the applied field. At present, the limiting angle appears to be about 40°, and the tracks become fainter as this limit is approached. The practical problems of obtaining larger angles for track-following, and reducing the variation in brightness, may eventually be clarified when the physical processes involved in spark formation are thoroughly understood.

Measurements have recently been completed at CERN [1] of the temporal development of track-following sparks, and an explanation of the observations was discussed in terms of space-charge fields arising from the interaction between electron avalanches which develop along the particle track (see Fig. 1). The object of the present work is to calculate, as accurately as possible, the temporal development of a track-following spark allowing for the inter-avalanche space-charge field, and to compare the results of these calculations with the experimental observations.

The differential equations for ionization growth in a distorted field are very difficult to solve and, in order to calculate the ionization growth exactly, numerical methods have to be used. The method of solving the differential equations is described in section 2, and in section 3 it is applied to the case of a large number of equally spaced avalanches.

1.1 Previous investigations

Several authors [2),3)] have performed numerical computations of ionization currents in distorted fields, but most of these investigations have been for one-dimensional geometry. That is, the densities and fields were assumed to be functions of x only. This is satisfactory

when applied to diffuse discharges between closely-spaced parallel plates, but not when used for single avalanches, or collections of avalanches. The field due to any element of volume in the discharge must fall off according to the inverse-square law at large distances. The one-dimensional equation :

$$\partial E/\partial x = K\rho$$

however, predicts no change at all in the electric field outside the charge distribution. In some recent work [4], the correct variation of field with distance has been obtained, while the ionization-growth equations have still been treated as one-dimensional.

All one-dimensional treatments fail eventually when the radial motion of the electrons (due to diffusion and drift in the distorted field) becomes comparable with their longitudinal motion. The method of calculation in such cases will now be discussed.

2. THE DIFFERENTIAL EQUATIONS AND BOUNDARY CONDITIONS

In the present work we shall define the field by the equation

$$\underline{E} = \text{grad } V$$

(instead of -grad V as usual). The purpose of this definition is to make the electron drift velocity $\underline{v}$ parallel with $\underline{E}$ and thus avoid the appearance of several negative constants in the equations.

Let n and N be the charge densities of electrons and positive ions respectively. Then, if recombination and photo-ionization effects are absent, we obtain [5]

$$\partial n/\partial t = \alpha vn - \text{div}(n\underline{v}) + D\nabla^2 n \qquad (1)$$

$$\partial N/\partial t = \alpha vn, \qquad (2)$$

where α and D are the ionization and diffusion coefficients of the electrons. The drift velocity of positive ions is less than 1/100 of the electron drift velocity, and for the purpose of the present inves-

tigation the ions may be considered stationary. The potentials are determined by Poisson's equation

$$\nabla^2 V = -K(N-n). \qquad (3)$$

When n and N are expressed in Coulomb.cm^{-3}, and $\nabla^2 V$ is in volt.cm^{-2} the constant K takes the value 1.131×10^{13}.

In addition, two empirical relations of the form

$$\alpha = \alpha(E)$$
$$\underline{v} = \underline{E}\,\mu(E)$$

give the dependence of α and $\underline{v}$ on the electric field.

Either of the following initial conditions may be used to start the calculation :

(a) At time t = 0, single electrons are present at various positions.

(b) At time $t = t_1$, the centre of each avalanche has moved a distance vt_1, and the negative charge density at a distance r from the centre is

$$n(r,t_1) = q_0(4\pi Dt_1)^{-3/2} \exp\left[\alpha v t_1 - \frac{r^2}{4Dt_1}\right].$$

Condition (a) is clearly simpler to write down, but is unsuitable to use in a numerical computation due to the difficulty of describing a very narrow distribution by a set of pivotal values.

Condition (b) is therefore used, with t_1 given such a value that the field distortion is negligible. q_0 is the charge on an electron, 1.6×10^{-19} Coulomb.

As a boundary condition on the potential, we require that it should represent a uniform field at large distances. The volume used in the calculation therefore depends on the rate at which the space-charge field decreases with distance. Since the avalanches may be approximated by dipoles, the field decreases as (distance)$^{-3}$, and so a fairly small volume may be used.

2.1 Finite-difference form of the equations

In the numerical computation, we must replace smooth distributions by sets of tabular values. The values are stored for a set of pivotal points. In the case of rectangular Cartesian coordinates, with

the points equally spaced in the three directions, the pivotal points are at the intersection of the planes

$$x = 0,\ H,\ 2H,..\quad y = 0,\ H,\ 2H,...\quad z = 0,\ H,\ 2H,...$$

The planes are numbered in succession, starting from (1,1,1) at the origin. Thus the point (I,J,K) is at $x = (I - 1)H$, $y = (J - 1)H$, $z = (K - 1)H$. H is called the mesh spacing.

2.1.1 The potential equation

If the potential distribution is sufficiently smooth so that terms like $H^2 \partial^4 V/\partial x^4$ are negligible compared with $\partial^2 V/\partial x^2$, then $H^2 \nabla^2 V$ may be approximated in finite difference form :

$$-6V(I,J,K)+V(I+1,J,K)+V(I-1,J,K)+V(I,J+1,K)+V(I,J-1,K)$$
$$+V(I,J,K+1)+V(I,J,K-1)$$

In the present work, the potentials are obtained by the method of relaxation. Suppose an approximate potential distribution $V_1(I,J,K)$ is known, then in general $H^2\left[\nabla^2 V_1+K(N-n)\right]$ will not be zero. The value of this expression gives the error in the approximate distribution V_1 at (I,J,K), and it is called the residual, R(I,J,K). The process of relaxation consists essentially of adjusting the potential at each point in succession in such a way as to make the residual there very small[6]. The particular advantage of the method of relaxation in the present application is that the charges (n and N) are changed by a small amount as the time is increased step-by-step, and so a reasonably accurate first approximation to the potential distribution is always available. The storage requirement is quite modest - only two tables (R and V) need be stored ; at least two would be required for any other method.

2.1.2 The ionization-growth equations

It should first be pointed out that the diffusion term in equation (1) is extremely small, for the pressures and times used in the present work. Very little error is introduced if we treat this process independently, to the first order of accuracy, simply adding

$\nabla^2 n \cdot D\Delta t$ on to every electron density after each time interval Δt. In order to simplify the account which follows, we shall therefore omit the diffusion term, although it is used, of course, in the computation. We shall consider the equation

$$\partial n/\partial t = \alpha vn - \mathrm{div}(n\underline{v}) \qquad (4)$$

together with the equation for the net charge density

$$\partial \rho/\partial t = \mathrm{div}(n\underline{v}). \qquad (5)$$

The positive ion density may be obtained, if required, from the relation $\rho = N - n$.

The equations (4) and (5) may be written

$$\partial n/\partial t = F(t) - G(t) \qquad (6)$$

$$\partial \rho/\partial t = G(t) \qquad (7)$$

$F \equiv \alpha vn$ and $G \equiv \mathrm{div}(n\underline{v})$ are scalar functions of position as well as time, and can be evaluated from the charge and potential distributions using simple second-order difference formulae.

Equation (6) may be integrated over an increment of time (to the first order of accuracy only) :

$$n(t+\Delta t) = n(t) + \left[F(t) - G(t)\right]\Delta t.$$

Second order accuracy is immediately obtained, however, if F and G are evaluated at time $t + \frac{1}{2}\Delta t$, and a convenient method of doing this is by linear extrapolation of the values already obtained for times $\leq t$. Thus :

$$F_1(t + \tfrac{1}{2}\Delta t) = \tfrac{3}{2} F(t) - \tfrac{1}{2} F(t - \Delta t)$$

assuming that the time-steps are equal. (It is very easy to generalise this formula for the case of unequal time-steps). Having obtained the first approximations, F_1 and G_1, we then find n_1, the first approximation to $n(t + \Delta t)$; a similar procedure yields the first approximation to the net density ρ_1.

The second stage of the iteration process consists of obtaining the potential distribution corresponding to the charges ρ_1, and hence the second approximations for F and G - $F_2(t + \Delta t)$ and $G_2(t + \Delta t)$ respectively. The second approximation for n is then

$$n_2(t + \Delta t) = n(t) + \tfrac{1}{2}\Delta t \left[F(t) + F_2(t + \Delta t) - G(t) - G_2(t+\Delta t)\right]$$

with a similar expression for ρ_2. One could continue this process and get third approximations, etc.., but it is better to choose the time-step so that sufficient accuracy is obtained with the second approximation, if possible. (If the first approximation is more than a few per cent in error, this indicates that third-order errors are becoming appreciable, and that the result would never be accurate, no matter how many iterations were used.)

Iterative methods generally require a fairly large amount of storage, but the programming is comparatively simple, especially as first-order interpolation (and extrapolation) in time is sufficient to give second-order accuracy in the charge densities. Also, a good estimate of the error is obtained as a by-product of the iteration process.

2.2 Method of calculation for a large number of equally-spaced avalanches

We have shown how to integrate the differential equations (1), (2), and (3) for the track-following spark, but we have not yet mentioned how the influence of neighbouring avalanches can be taken into account. At first sight, it would seem that we must deal with 2, 3 or more avalanches simultaneously, but by suitable choice of the boundary conditions all calculations may be done with one avalanche only, as will now be explained.

The avalanche is initially contained in a rectangular volume, with thickness equal to the spacing between the avalanches, a, (see Fig. 2), and the coordinates of the pivotal points are specified with respect to axes inclined at an angle to the applied field. The x-axis is parallel with the track, the z-axis is perpendicular to the

track and to the applied field, and the y-axis completes the usual rectangular system. In the calculation, it is convenient to separate the external field from that of the avalanches ; thus, in the solution of $\nabla^2 V = -K\rho$, the potentials refer to the avalanche field only. This enables us to write down the boundary conditions on the potentials in the simpler form :

$$V = 0 \quad \text{for} \quad y = 0, \quad y = b, \quad z = -c, \quad z = +c,$$

where $z = 0$ is a plane of symmetry. The surfaces $y = 0$, b and $z = \pm c$ have to be sufficiently far away to cause negligible perturbation of the avalanche fields.

The faces $x = 0$ and $x = a$ are not boundaries in the usual sense. The potentials and fields, at corresponding values of y and z, are required to be the same on both faces, so that a point in $x = a$ (regarded as a neighbour of the corresponding point in $x = 0$) is no different from any point inside the volume.

(These boundary conditions are similar to those for Poisson's equation inside a conducting torus. Not only must the potentials on the surface be zero, but the solution must also be periodic around the torus.)

Having obtained the potential distribution, we have only to differentiate with respect to x, y and z, and add the components of the applied field $-E\cos\phi$, $E\sin\phi$, 0.

By requiring that the charge densities also are the same on the surfaces $x = 0$ and $x = a$, we may allow for the merging of the initially separate avalanches.

3. RESULTS

3.1 Empirical formulae

All the calculations were carried out using data for pure neon at $E/p \sim 10$ V cm^{-1} torr^{-1}. Measurements of the primary ionization coefficient over the range of interest have been obtained by Kruithof [7], and were found to fit the formula

$$\frac{\alpha}{p} = 6.6 \times 10^{-4} \times \left(\frac{E}{p} - 1.42\right)^2 \text{ (cm torr)}^{-1}, \quad \left(\frac{E}{p} \geq 1.42\right).$$

The electron drift velocity, on the other hand, has only been measured for much smaller values of E/p. These measurements, collected by Healey and Reed [8], are closely approximated by

$$v = 3.39 \times 10^6 \times \left(\frac{E}{p} - 1.5\right)^{\frac{1}{2}} \text{ cm s}^{-1}, \quad \left(\frac{E}{p} \geq 1.5\right)$$

and it was assumed that this formula could be used as a basis for extrapolation to higher values of E/p. When values of αv were calculated at $E/p \sim 10$, however, they were found to disagree with the measurements of Caris et al. [1], being about 30% too large. It was assumed that the experimental values of α could be relied upon, while the formula for extrapolating v was in error. (It is likely that the extrapolated v will be too large, due to the larger amount of energy lost in ionizing collisions at higher E/p.) In the absence of reliable mobility data at large E/p, it was decided to adjust the above values by a constant correction factor, giving

$$v = 2.6 \times 10^6 \times \left(\frac{E}{p} - 1.5\right)^{\frac{1}{2}}$$

and this formula was used in subsequent calculations.

Values of the diffusion coefficient D were again deduced from data given by Healey and Reed, and the pressure variation was assumed to be of the form

$$D = 9.86 \times 10^6/p \text{ cm}^2 \text{ s}^{-1}.$$

3.2 Preliminary investigations for single avalanches

Only a few results will be given here, for the purpose of comparison with track-following sparks. It is hoped to extend the investigations to other gases - notably air, because of the great technological importance of air as a high-voltage insulator. The results of these further investigations will be reported elsewhere.

Because of the axial symmetry of a single avalanche, the equations could be expressed in cylindrical polar co-ordinates, thus reducing the problem to a two-dimensional one. It was also possible to use simpler boundary conditions on the potential distribution.

Figure 3 shows the ~~temporal variation~~ of current and instantaneous light intensity for a single avalanche at $p = 690$ torr, $E = 6.73$ kV cm^{-1}. The current plotted is the average current over a one-cm interval containing the avalanche. (The peak current in the avalanche will be considerably greater.) The light output is assumed to be proportional to the rate of ionization [9]. The units are arbitrary (since the signal recorded in practice depends on the size and quality of the optical components), but the scale was chosen so as to make the intensity numerically equal to the current at small times (i.e., in uniform fields). Thus it can more easily be seen whether the light intensity is increasing faster than the current, or vice versa.

It can be seen that the gradients of both curves fall slightly at 76 ns, and begin to rise again at about 90 ns. The initial fall in the gradient is because the average field in the electron cloud is decreased by the dipole field of the avalanche. The subsequent rise follows when the increase in the ionization coefficient α at the front of the electron cloud more than compensates for the decrease in α elsewhere. This increase in gradient depends on the detailed form of the dependence of α on E, and is only expected to occur at comparatively low values of E/p. It is not yet certain whether the initial decrease in the gradient will occur for all gases and pressures ; this will be the subject of further investigations.

Figure 4 shows the variation of electric field along the axis of the avalanche at various times. The field is decreased near the centre of the avalanche and increased at the front. The distribution of electron velocity in the avalanche is therefore such as to spread it out lengthways. The field at the centre of the avalanche appears to attain a stationary value at later times. The rate of ionization in this region almost exactly cancels out the loss of electrons due to drift and diffusion, leading to a region of almost uniform density, moving forward and lengthening.

The distribution of field, although of great importance in the calculation, is not amenable to experimental observation. Graphs of light intensity along the axis are therefore plotted in Fig. 5. This diagram shows how the luminosity is restricted to a small region at the front of the avalanche. The second maximum appearing at the back of the avalanche is due to the rapid increase in field there (see Fig. 4).

Each of the curves in Fig. 5 could be obtained in practice by taking a photograph of the avalanche with a very short exposure. Another device commonly used to observe rapidly-moving phenomena is the streak camera, in which the avalanche would be observed through a slit parallel with its axis, while the image is swept across the film in the direction perpendicular to the slit. The result is to record on the film the motion of regions of equal intensity. For the results of Fig. 5, the corresponding streak-camera pictures are plotted in Fig. 6. Which of the curves is in fact observed depends on the sensitivity of the camera. The arrow in Fig. 6 represents the drift velocity of the electrons in a uniform field, while the region of maximum brightness moves forward as indicated by the dotted line, attaining a speed many times greater than the electron drift velocity. The subsequent behaviour of the second maximum will be affected very much by the production of secondary electrons (whether they arise from electrode effects, the photo-detachment of negative ions, or any other process), and so will be expected to depend critically on the details of the experiment.

3.3 Investigations of the track-following spark

3.3.1 The track-following process

Figures 7 and 8 show the distributions of electron density and lines of force for two different times. The gas is neon at 690 torr, the field is 6.73 kV/cm, and the avalanche separation is 2 mm, along a track inclined at 30° to the applied field. In the first diagram ($t = 82.8$ ns), the field is only slightly distorted, but already the avalanches have become asymmetrical and have started to bend towards the track direction. In the second diagram ($t = 97.9$ ns) the field lines follow the track very closely, and the avalanches have merged to form a continuous tube of current.

A better idea of the track-following action may be obtained by plotting the direction of the resultant current against time. The angle between the current and the applied field, θ say, is initially zero, and increases gradually as the current vector rotates. By repeating the computation with different track-angles ϕ, and plotting θ/ϕ against time, we may compare the relative rates of rotation of the current. This is done in Fig. 9, with avalanches 1 mm apart. It will be noticed that the relative rotation depends strongly on the track angle ; the values of θ/ϕ at $t = 90$ ns change by a factor of 3 as θ goes from 60° to 30°. The solid curves in Fig. 9 are obtained using published values of the diffusion coefficient [8]. To test the influence of D, the calculation for $\phi = 30°$ was repeated with D halved. The current was found to rotate much faster, as can be seen from the dotted curve in Fig. 9.

Figure 10 shows 3 curves obtained at a higher pressure ($p = 1380$ torr), but at the same E/p. (It was assumed that the number of initial ion-pairs would be doubled also.) The rotation of current now proceeds at a greater speed, but the dependence on angle is also greater.

These results indicate that track following occurs, to a varying extent, for all angles. The value assumed for the diffusion coefficient is seen to have a very great effect. It is important, therefore, that an accurate value of D should be measured under the conditions of the present experiment (i.e., when new electrons of low energy are continually being generated by ionization).

3.3.2 Variation of light intensity

In calculating the light-output, the excitation coefficient was again assumed to be proportional to α, and the scale was chosen so as to make the light-output and current equal in magnitude in an undistorted field.

Figure 11 shows the temporal growth of intensity for various track angles. There is a strong dependence on angle, as observed experimentally (see Fig. 5, Ref. [1]), but the slopes of the experimental curves are greater in the later stages.

3.3.3 Further development of the spark

In an attempt to explain the increase in slope of the experimental curves, a calculation was made with α and v adjusted slightly, but with the product αv kept constant. Curve A in Fig. 12 shows the result of increasing α by 20% (and reducing v). Curve B is the same as in Fig. 11 (at 30°). Curve C is the result of increasing v by 20% (and decreasing α). The difference between the curves is not very great, and so the error introduced by our extrapolation of the drift velocities quoted by Healey and Reed is not serious.

It is known that the effective ionization coefficient in the inert gases increases with current density. This is due to the high potentials of some of the excited states (80 to 90% of the ionization potential), and to their relatively long lifetime. Thus if an excited atom is struck by a low-energy electron, it stands a good chance of being ionized. For neon at $E/p \sim 10$, it is expected [10] that the excited atom density is about 10 times the electron density n. The

collision frequency for a 10 eV electron is about 5×10^{12} s^{-1}, and so the number of collisions per unit time per unit volume between electrons and excited atoms is $5 \times 10^{12} \times n \times 10n/(3 \times 10^{19}) = 1.6 \times 10^{-7}$ n^2. The curve D in Fig. 12 was calculated assuming an extra ionization term of 8×10^{-4} n^2 and, although it agrees quite well with the experiment, it is very difficult to justify the assumption of such a large ionization effect.

One must eventually consider electrode effects. When the current density in the spark reaches about 1 A cm^{-2} (as in the present calculations), the spark may be considered as a low-resistance conducting channel, which extends from the anode to a point a few mm from the cathode. The passage of current along the spark and into the anode will raise the potential at the other end, producing a very large field between the spark and the cathode (about 10 to 100 times the applied field). Although this may not be large enough to induce field-emission, any electrons emitted by the photo-electric effect will ionize extremely rapidly, bridging the samll gap between the spark and the cathode, and producing a very dense cloud of electrons. The new supply of electrons enables a wave of ionization to spread at an increased rate along the spark, and conditions for an arc discharge develop, characterized by a large current density ($\sim$ several kA cm^{-2}) and the collapse of voltage. Under these conditions, the two-stage ionization of already excited atoms becomes a decisive factor, and the spark is constrained to flow along the same channel.

4. CONCLUSIONS

We have succeeded in computing the development of a track-following spark up to the stage where electrode-effects or two-stage ionization processes have become important. It has been found in all cases that there is a tendency for the current to rotate into the direction of the track. The failure to track-follow under certain conditions must therefore be attributed to some other process which

we have been unable to take into account. A possible disturbing effect arises from the statistical nature of ionization. If one avalanche gets ahead of its neighbours, it may be pulled across to the anode, escaping from the local field in the track. The probability of doing so clearly increases with the track angle. Thus, for large angles, a number of small sparks will be observed to jump across from the track to the anode. On the other hand, for large track angles, a larger area of the cathode will be irradiated with photons from the spark, and a larger area will also be subject to an increased field. Sparks will therefore jump across from the cathode to the track, and so the track-following action will be distorted at both ends.

The computation of the growth of current in an inclined spark, allowing for electrode effects, is evidently an extremely long and difficult problem, and will probably not be undertaken for some time. Some of the characteristics of the final stages of breakdown, however, may be deduced from calculations for sparks which are parallel with the field. For example, the temporal growth of current in a spark of inclination ϕ in a gap of width d will be approximately the same, in the later stages, as for a normal track in a gap of width $d/\cos\phi$, with the same potential between its plates. If we restrict our attention to normal sparks, the problem becomes two-dimensional, and is suitable for computation. Such calculations will form part of the more extensive investigation of single avalanches, which is being undertaken at present.

5. ACKNOWLEDGEMENTS

I am very grateful for the invitation I received to undertake this line of work during a period of three months as visiting scientist at the NPA Division, CERN. May I thank Berend Kuiper, Laurens Caris and Malcolm Williams, who are engaged in this work, for their many interesting discussions, and also other members of NPA Division for their interest and encouragement.

6. REFERENCES

1) L. Caris, B. Kuiper and E.M. Williams - Characteristics of electrical breakdown along particle trajectories in a wide gap spark chamber, CERN NPA/Int. 67-13.

2) A.L. Ward - J.App.Phys. 36, 2540 (1965).

3) H. Schlumbahn - Z. Naturforschung 22a, 1257 (1967).

4) A.J. Davies, C.J. Evans and F. Llewellyn Jones - Proc.Roy.Soc. A.281, 164 (1964) ;
C.G. Morgan, C.J. Evans, W.T. Williams and A.J. Davies - Brit.J.App.Phys. 16, 494 (1965).

5) C.G. Morgan - Fundamentals of electric discharges in gases, Handbook of vacuum physics, Oxford, Pergamon Press (1965).

6) A.J. Davies and C.J. Evans - Proc.I.E.E. 114, 1547 (1967).

7) See L.B. Loeb - Basic processes of gaseous electronics, University of California Press, Berkeley (1955).

8) R.H. Healey and J.W. Reed - The behaviour of slow electrons in gases, Amalgameted Wireless, Sydney (1941).

9) Recent unpublished work by W.R.L. Thomas, University College of Swansea, indicates that the excitation coefficient is almost proportional to the field, but this is not expected to make a very great difference to the results.

10) W.R.L. Thomas - private communication.

7. FIGURE CAPTIONS

Figure 1 — The initial stages of avalanche growth on an ionized track.

Figure 2 — A rectangular cell containing one avalanche.

Figure 3 — Current and light intensity curves for a single avalanche. Neon gas ; p = 690 torr ; E = 6.73 kV/cm.

Figure 4 — Field distribution in a single avalanche for the following times : 77.7, 79.9, 81.5, 82.9, 84.2, 85.3, 86.4, 87.4, 88.5, 90.5, 91.5, 92.5, 93.5 ns.

Figure 5 — Distribution of light intensity along the axis of a single avalanche at various times.

Figure 6 — Curves of Fig. 5 re-plotted to show expected streak camera patterns. Light intensity (arbitrary units) marked on curves.

Figure 7 — Field lines and electron-density contours during the development of a track following spark. Neon gas ; p = 690 torr ; E = 6.73 kV/cm ; track angle = 30°, avalanche separation = 2mm, time = 82.8 ns.

Figure 8 — Data as for Fig. 7 at time = 97.9 ns.

Figure 9 — Rotation of current vector into the track direction. Neon gas ; p = 690 torr, E = 6.73 kV/cm, avalanche separation = 1 mm. Dotted curve : ϕ = 30°, diffusion coefficient halved.

Figure 10 — Rotation of current vector into the track direction. Neon gas ; p = 1380 torr ; E = 13.46 kV/cm ; avalanche separation = 0.5 mm.

Figure 11 — Light output (arbitrary units) for various track angles. Neon gas ; p = 690 torr ; E = 6.73 kV/cm, avalanche separation = 1 mm.

Figure 12 — Light output for track angles of 30°. B - same data as Fig. 11. A - α increased by 20% ; v decreased C - v increased by 20% ; α decreased D - same as B, but with a non-linear ionization term.

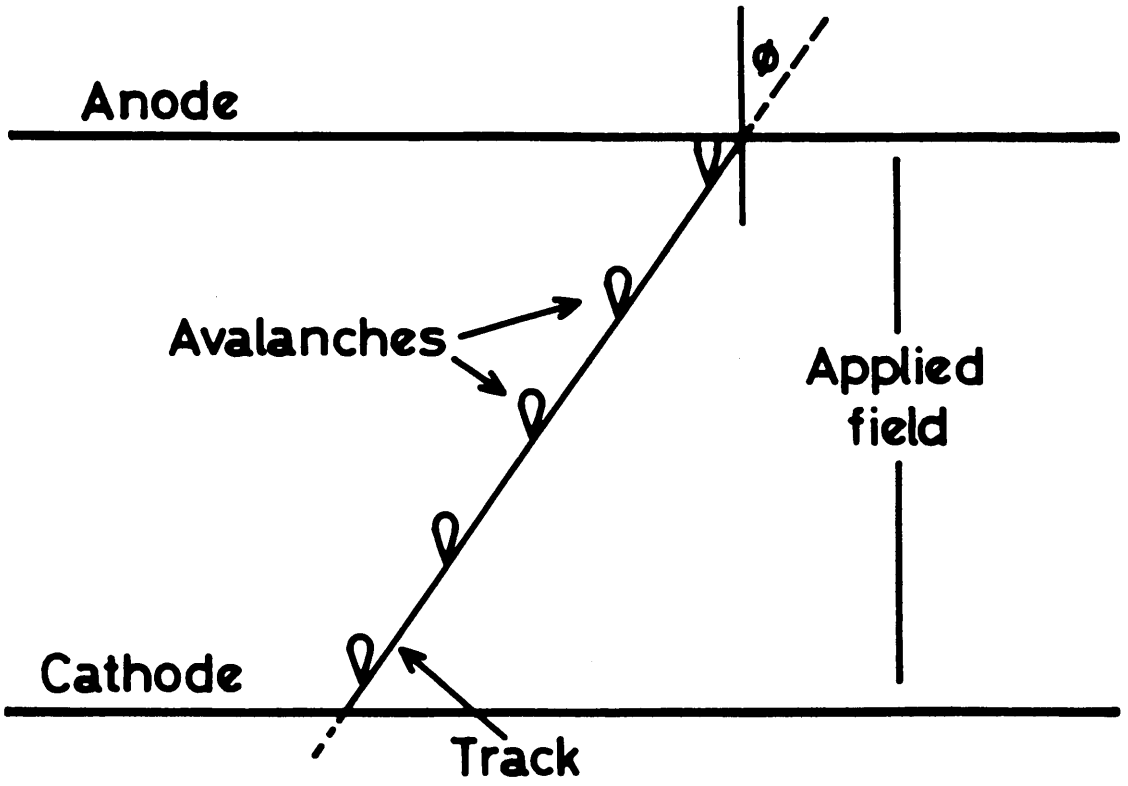

Fig. 1 The initial stages of avalanche growth on an ionized track.

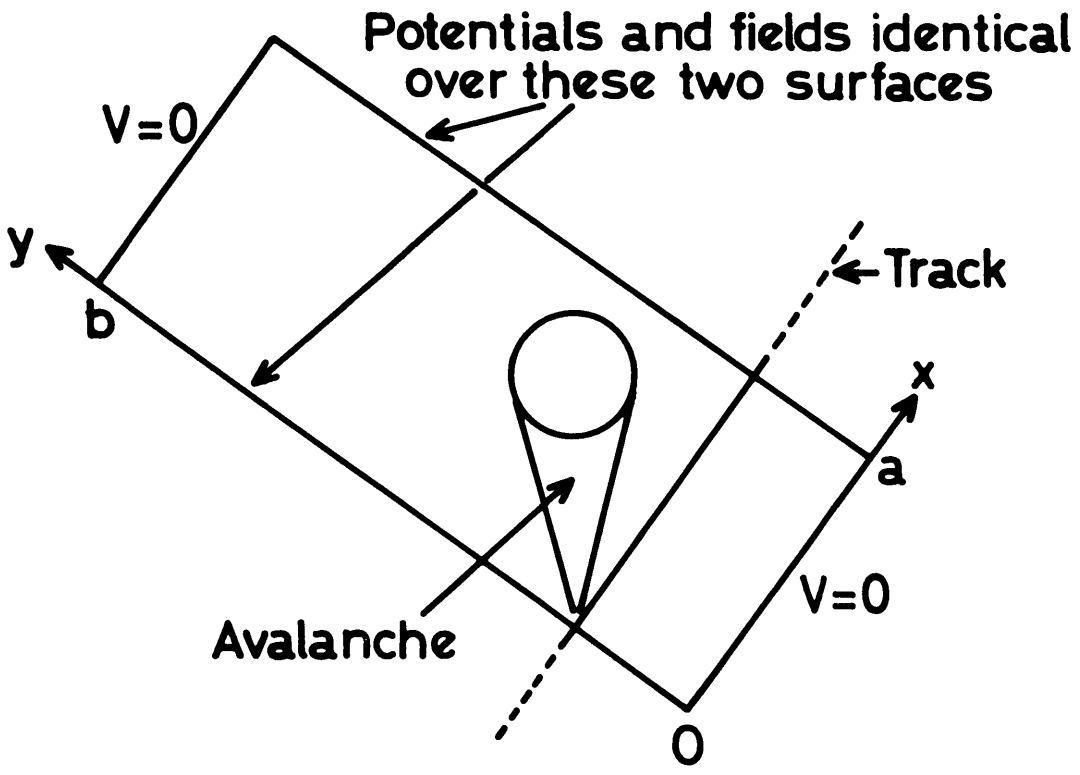

Fig. 2 A rectangular cell containing one avalanche.

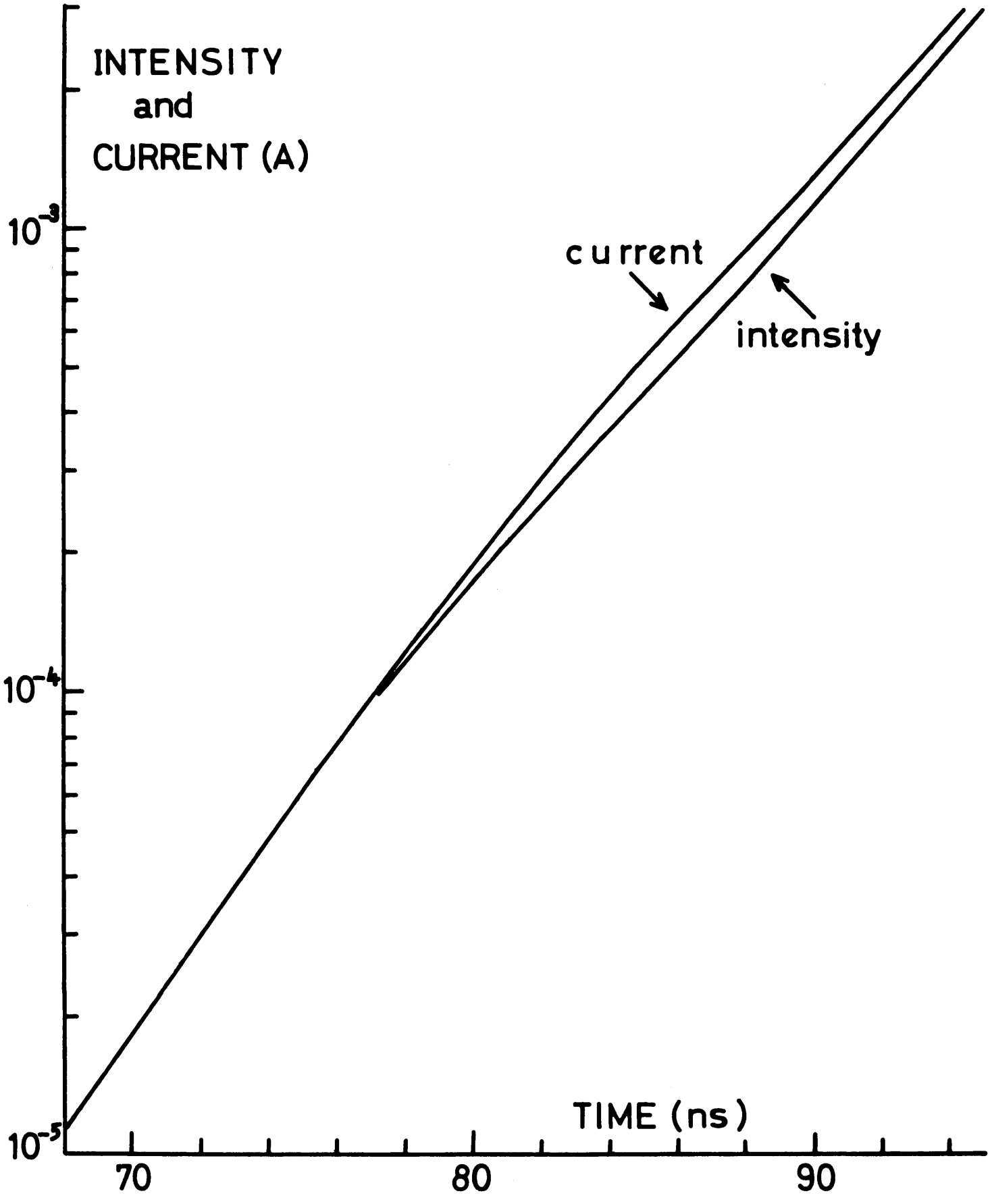

Fig. 3 Current and light intensity curves for a single avalanche. Neon gas; p = 690 torr; E = 6.73 kV/cm.

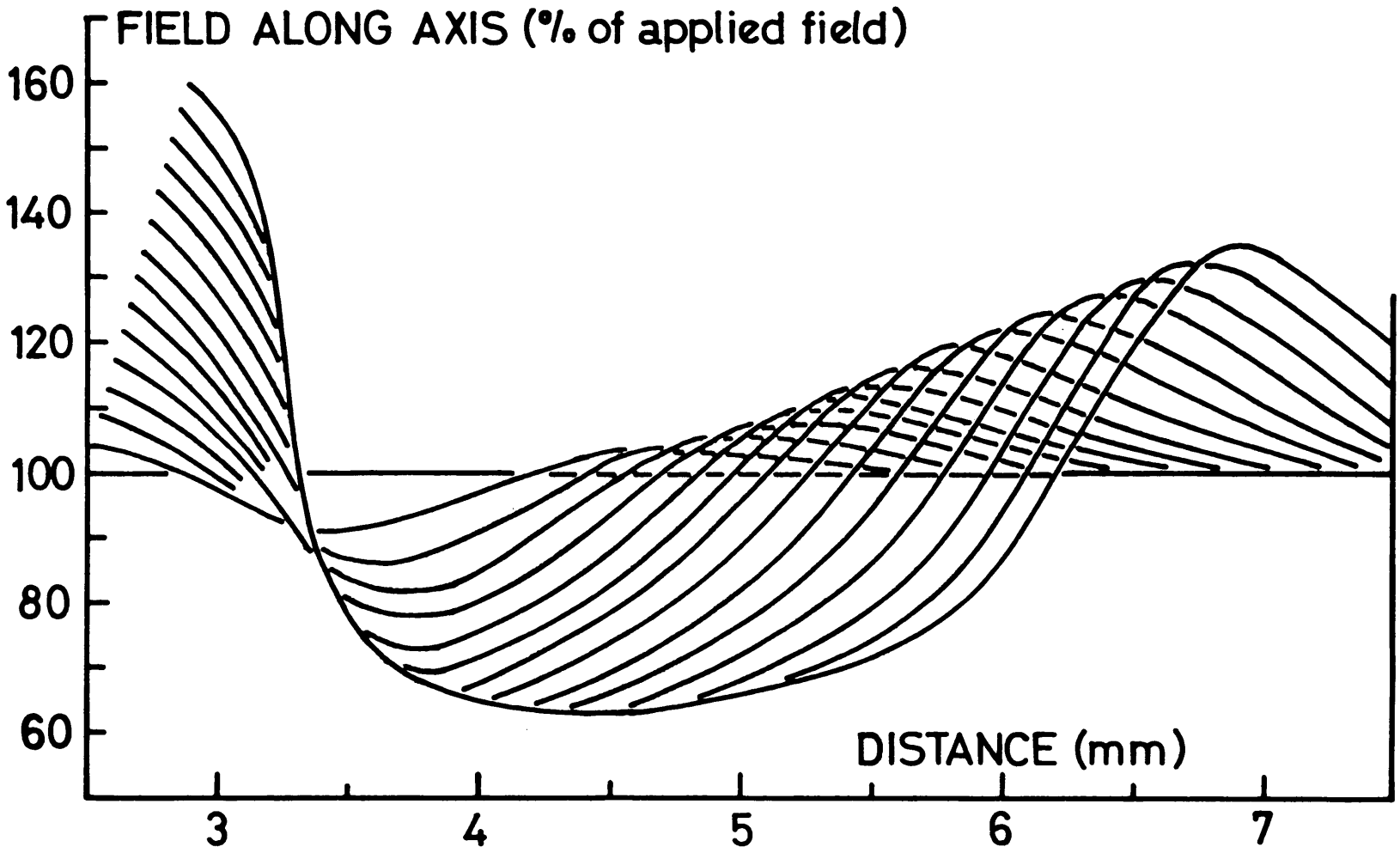

Fig. 4 Field distribution in a single avalanche for the following times : 77.7, 79.9, 81.5, 82.9, 84.2, 85.3, 86.4, 87.4, 88.5, 90.5, 91.5, 92.5, 93.5 ns.

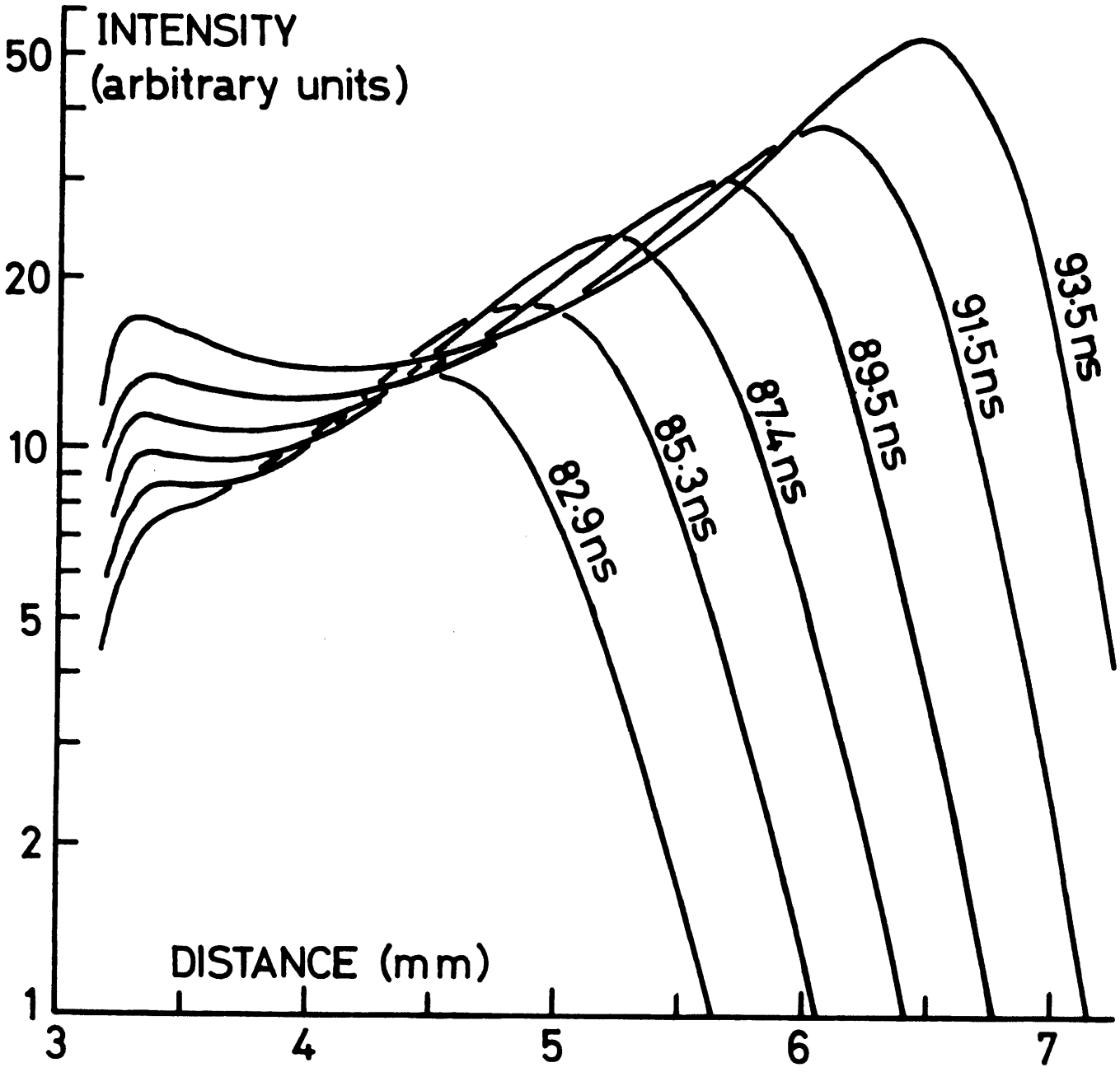

Fig. 5 Distribution of light intensity along the axis of a single avalanche at various times.

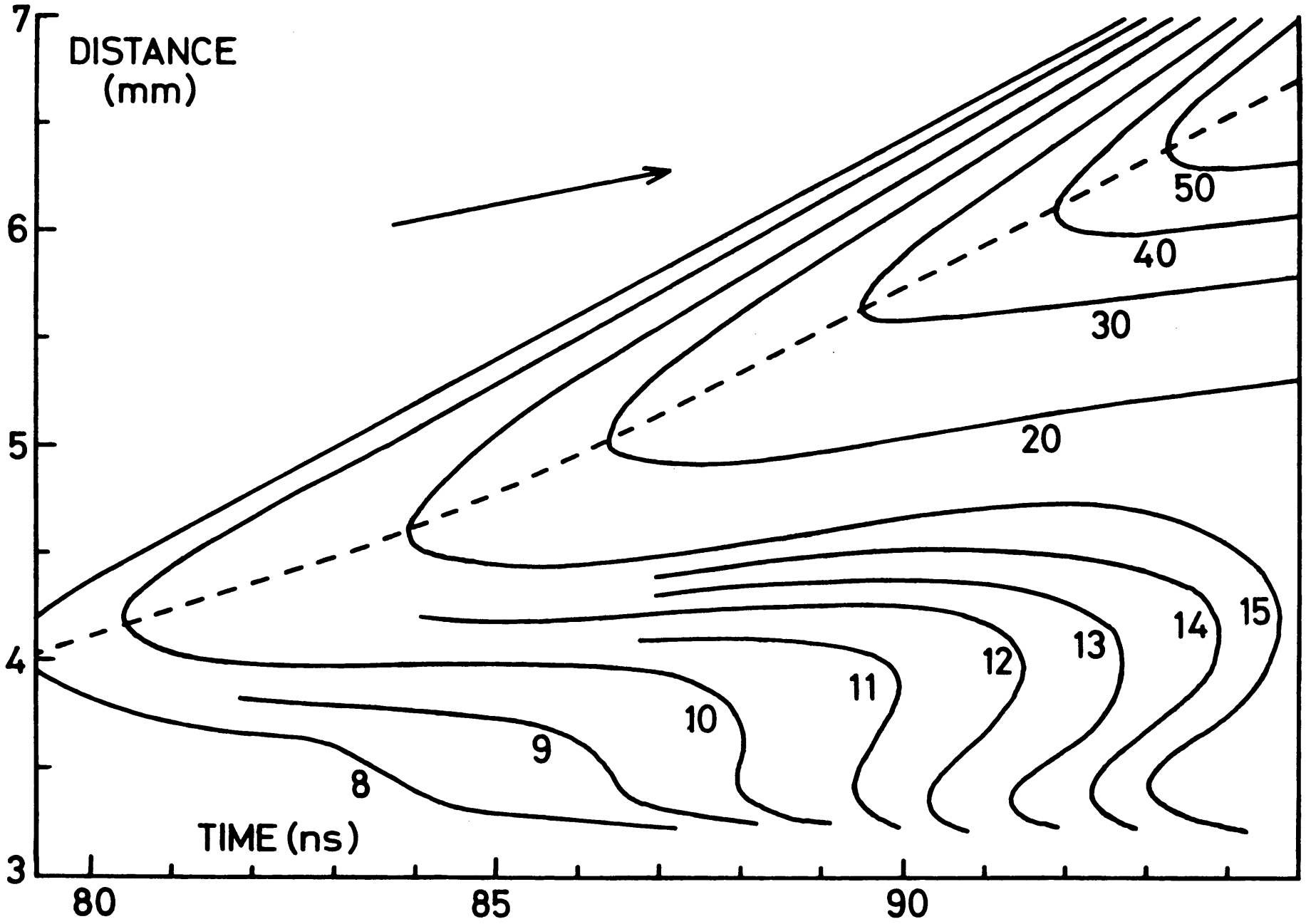

Fig. 6 Curves of fig. 5 re-plotted to show expected streak camera patterns. Light intensity (arbitrary units) marked on curves.

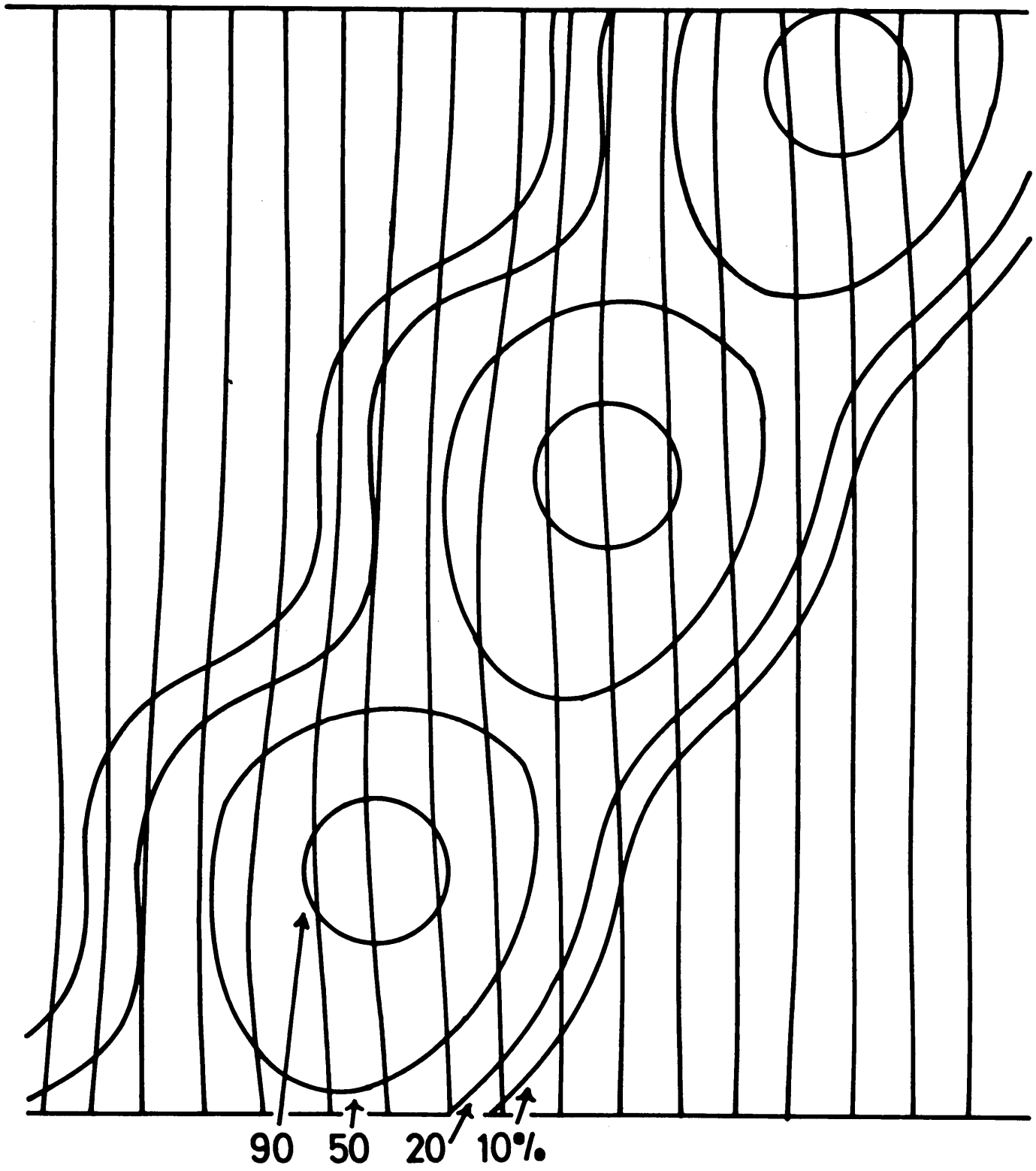

Fig. 7 Field lines and electron-density contours during the development of a track following spark. Neon gas; p = 690 torr; E = 6.73 kV/cm; track angle = 30°, avalanche separation = 2 mm, time = 82.8 ns.

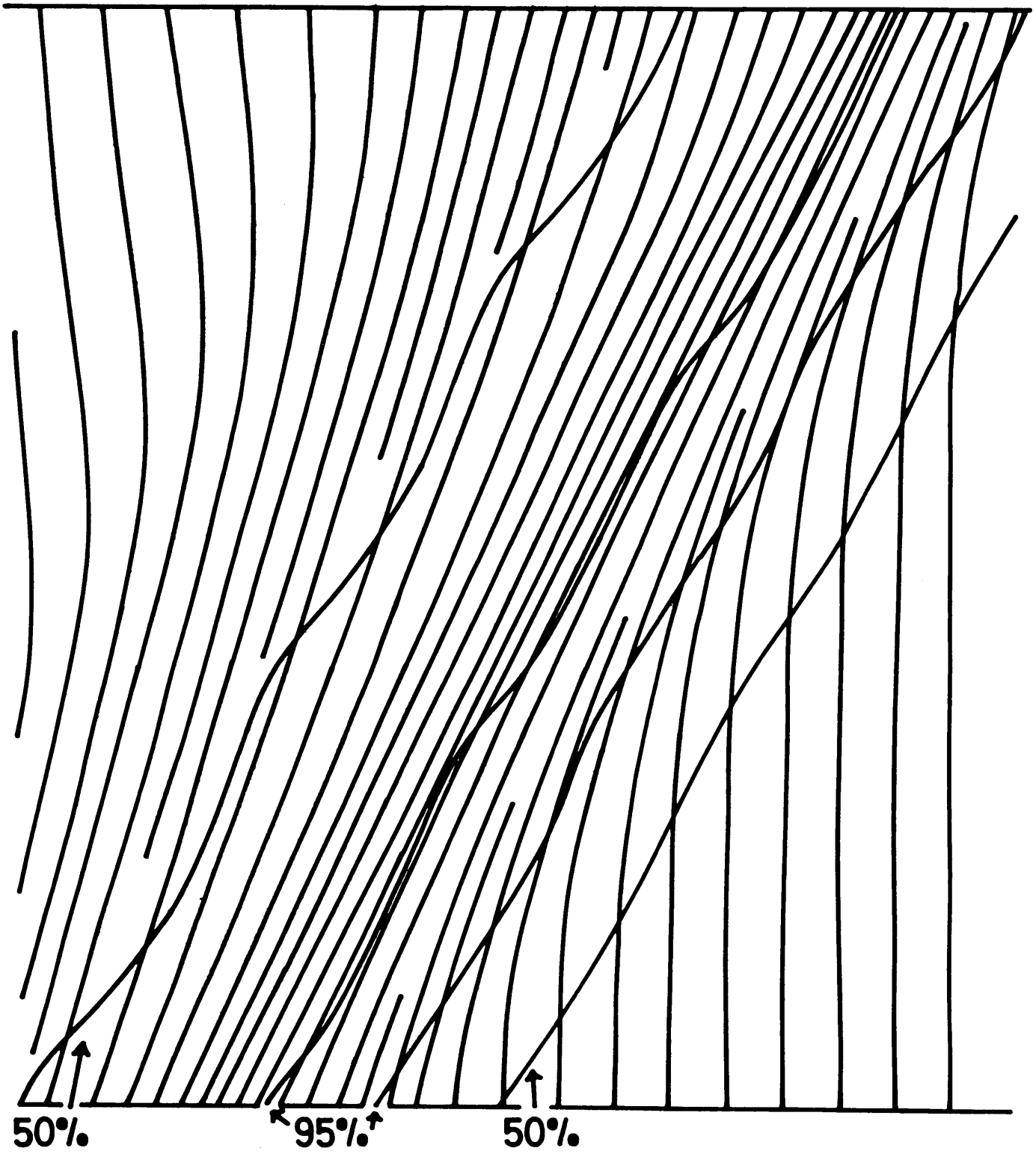

Fig. 8 Data as for fig. 7 at time = 97.9 ns.

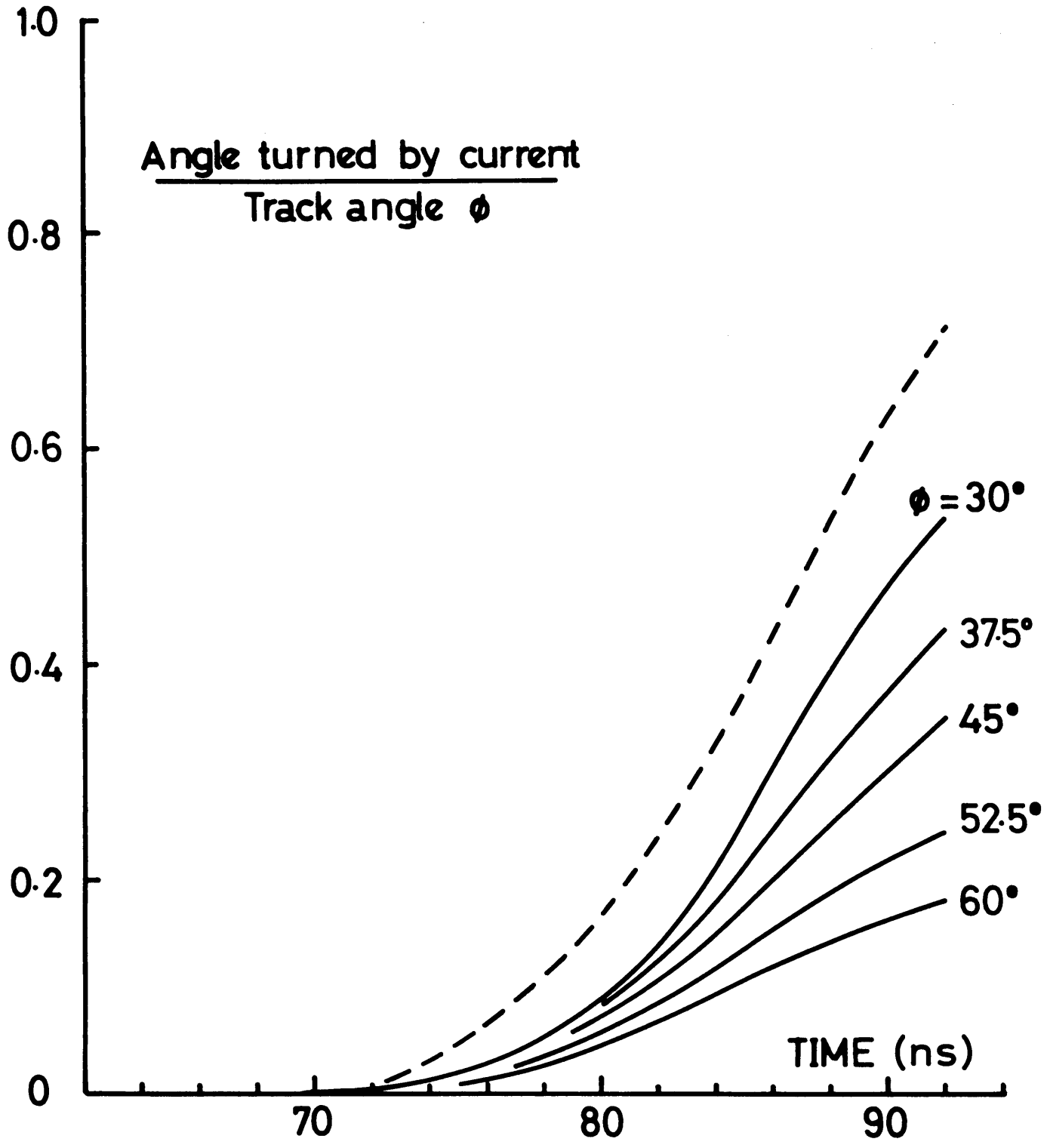

Fig. 9 Rotation of current vector into the track direction. Neon gas; p = 690 torr, E = 6.73 kV/cm, avalanche separation = 1 mm. Dotted curve: $\phi = 30^{\circ}$, diffusion coefficient halved.

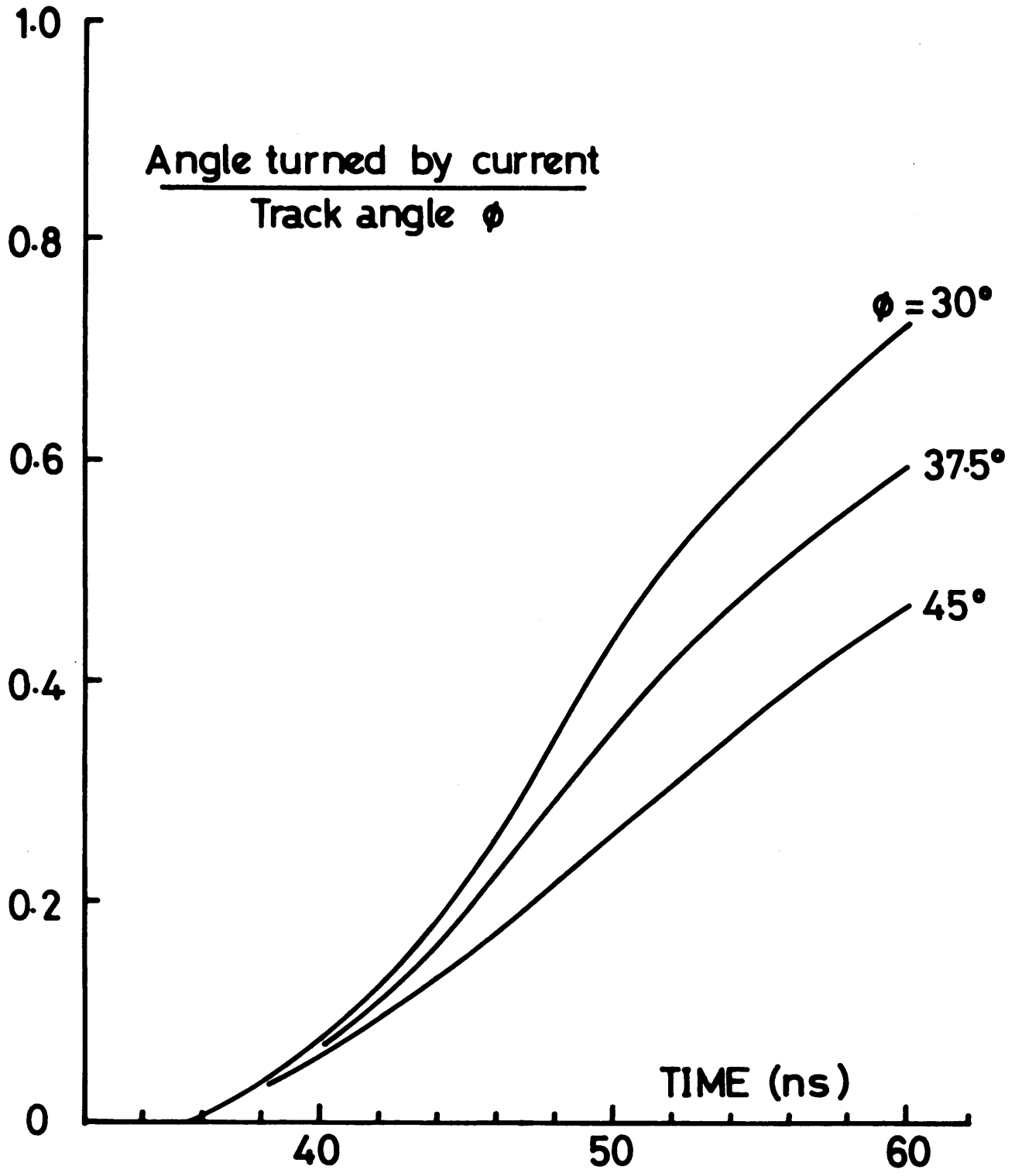

Fig. 10 Rotation of current vector into the track direction. Neon gas; p = 1380 torr; E = 13.46 kV/cm; avalanche separation = 0.5 mm

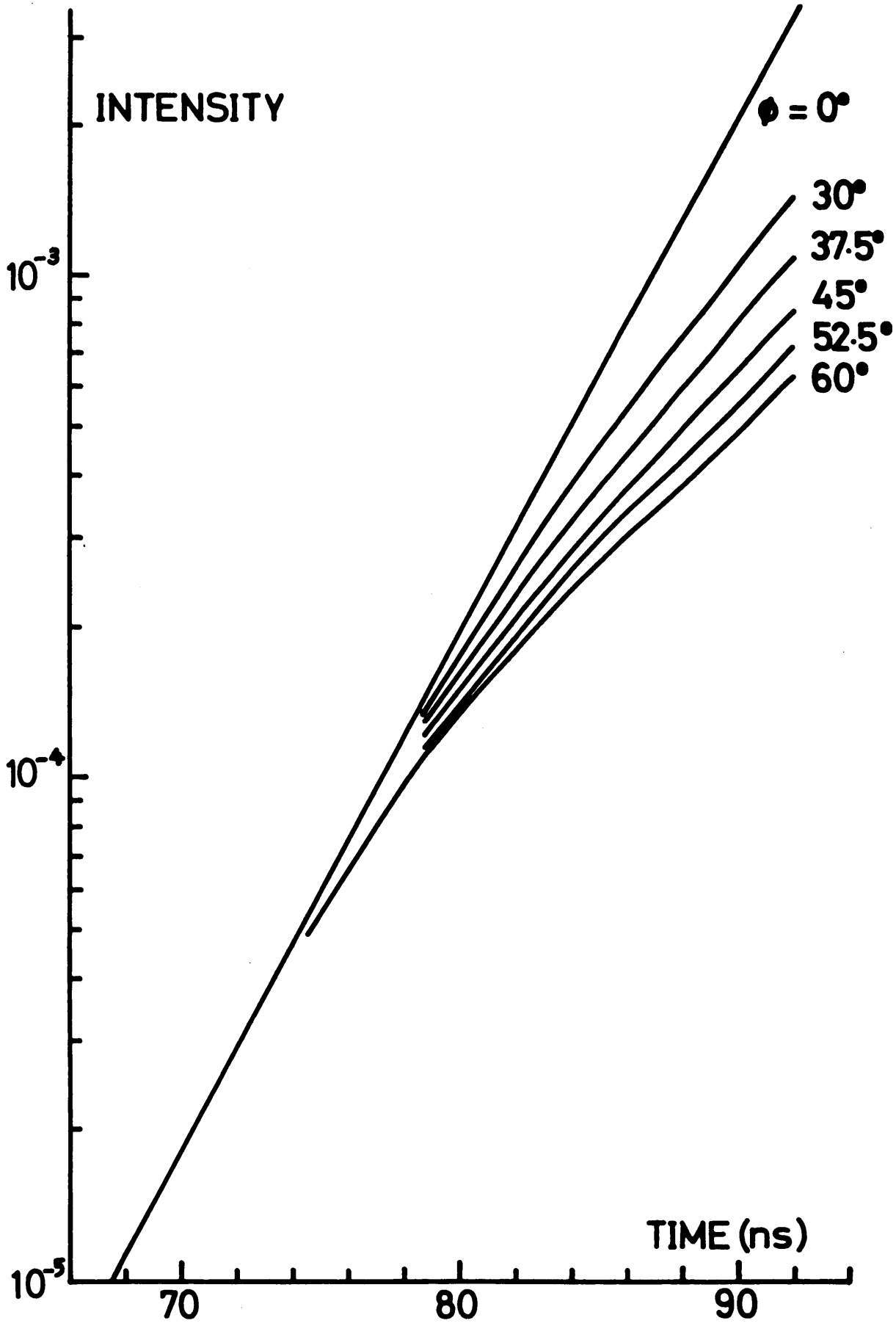

Fig. 11 Light output (arbitrary units) for various track angles. Neon gas; p = 690 torr; E = 6.73 kV/cm, avalanche separation = 1 mm.

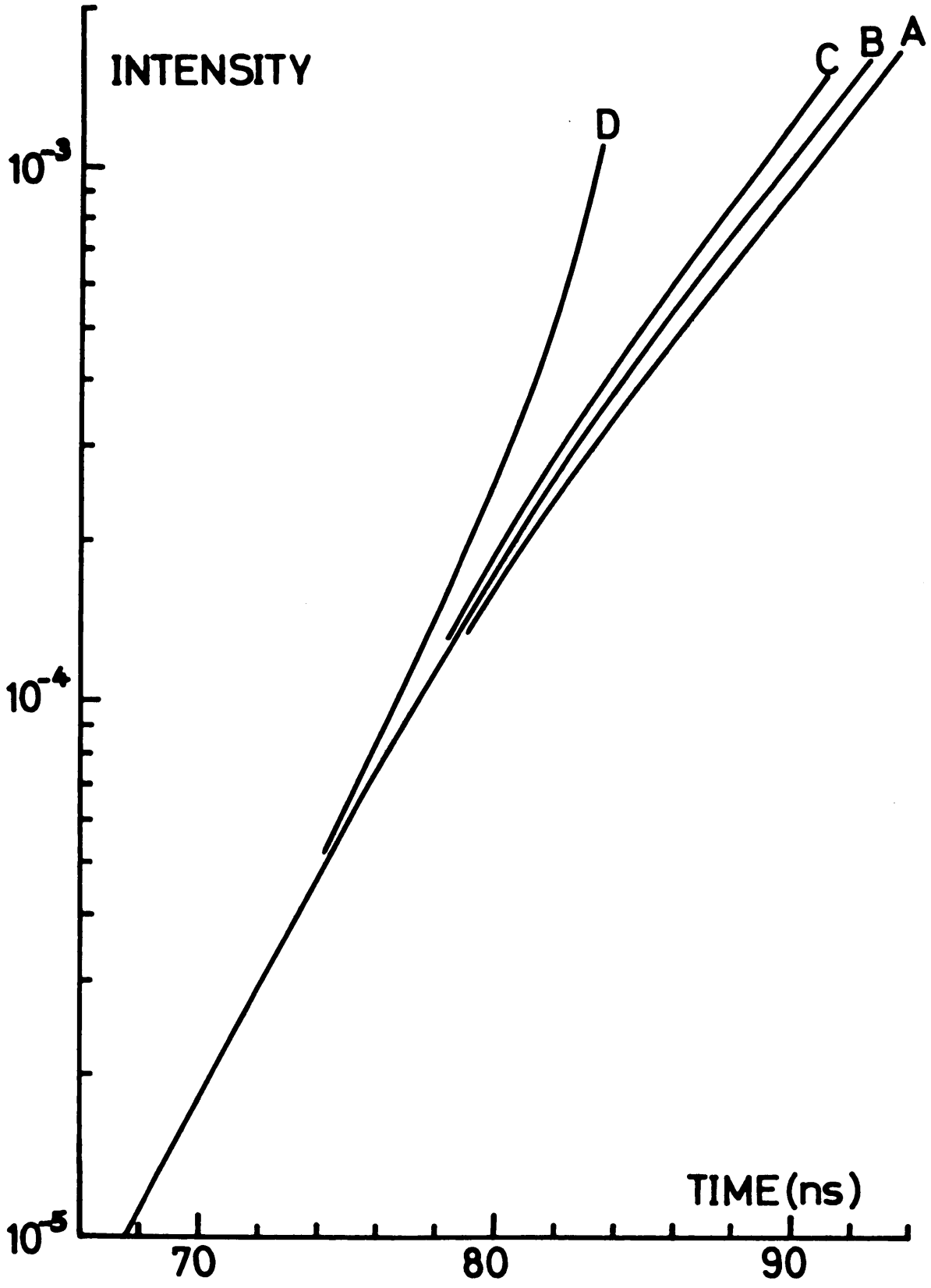

Fig. 12 Light output for track angles of 30°. B - same data as fig. 11. A - α increased by 20 %; v decreased. C - v increased by 20 %; α decreased. D - same as B, but with a non-linear ionization term.